Chromespinel and Magnetite as Indicators for Recognition of Genesis and History of Serpentinites in Baft Ophiolite Mélange (Kerman Province in Iran)

N. Mohammadi[*] and H. Ahmadipour

Department of Geology, Faculty of Science, Shahid Bahonar University of Kerman, Kerman, Islamic Republic of Iran

Abstract

Baft ophiolite mélange is a part of Naein-Baft ophiolite (southeast of Kerman province in Iran). Serpentinites from Baft ophiolite mélange contain different types of spinels such as chromite, chromespinel, ferritchromite and magnetite which can reveal different stages of evolution in host serpentinites. The compositions of Baft chromites show that they belong to podiform chromitites that may have crystallized from boninitic magmas. It seems that the Baft chromitite ores initially have been formed in a primary ophiolitic complex within dunitic envelopes; In the next stage, due to serpentinization of the peridotites and ascending of the resulted serpentinite, the studied deposits have been emplaced along the shear zones of the Baft ophiolitic melange. The compositions of primary Cr-spinels show that the Baft ophiolite has been formed in a suprasubduction zone in an arc/back-arc environment and the host rocks represent serpentinized Alpine type mantle residual peridotites. These studies suggest that the first serpentinization has taken place in an ocean floor environment and in this stage, mesh-textured serpentinites formed under static conditions. Then, the main serpentinization occurs and Cr-spinels have progressively replaced by ferritchromite rims, probably due to regional metamorphism. It seems that in the studied area, flare-textured serpentinites have passed higher temperature and pressure, and their formation can be related to dynamic evolutions such as subduction of Naein-Baft oceanic slab beneath the central Iranian microcontinent. Probably, the formation of magnetite fibers (type II) have accompanied by deformation process, while idiomorphic magnetites (type I) have produced from the passing Fe-rich fluids.

Keywords: Baft ophiolite mélange; Chromite; Iran; Magnetite; Serpentinite

Introduction

Serpentinization and deserpentinization processes recycle matter from the mantle to the crust and back to the mantle, through the states of fertile peridotite, residual harzburgite, serpentinized oceanic crust, subducted and obducted ophiolites. Because they contain traces of that history, serpentinites deserve
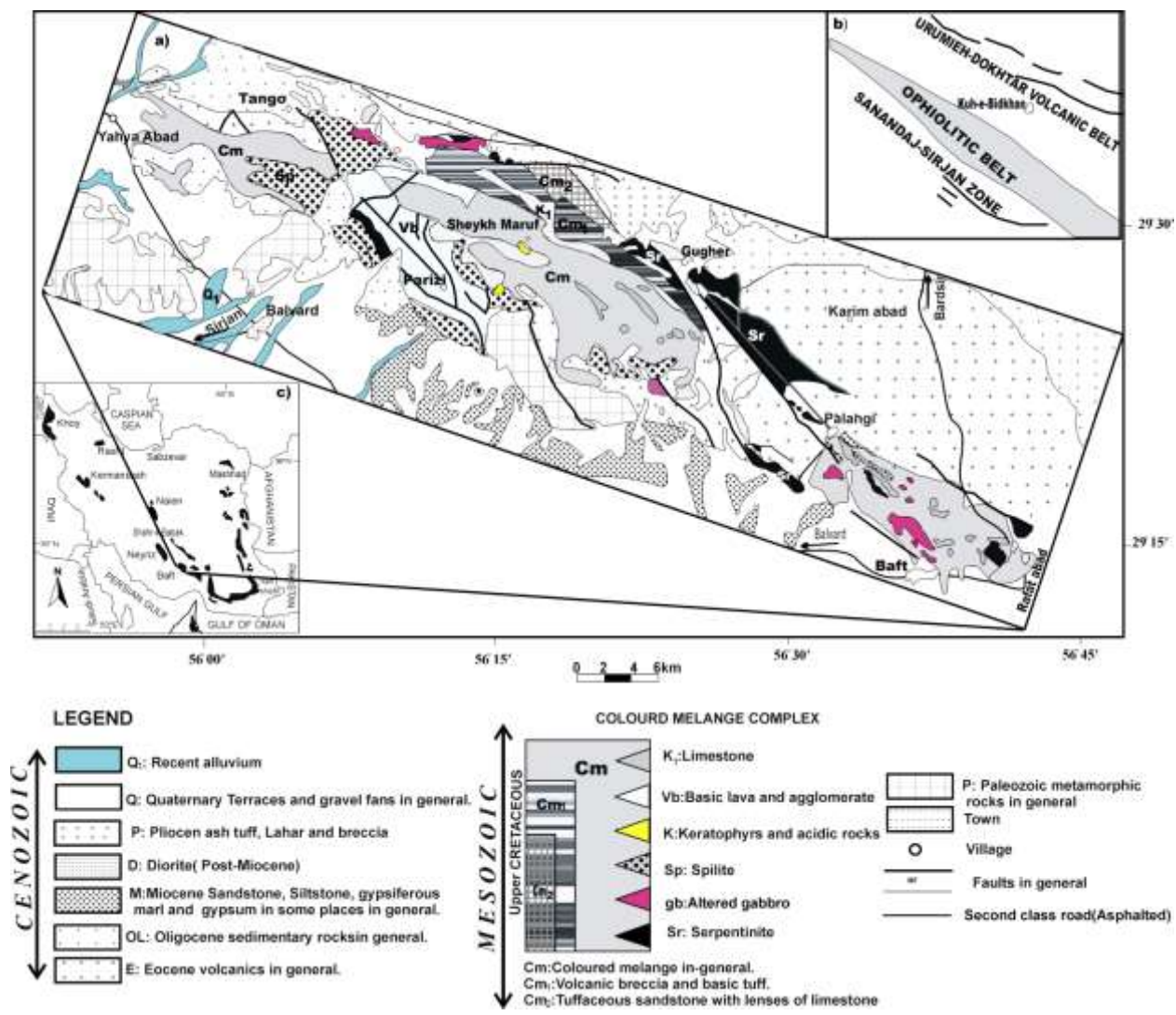

Figure 1. a) Geological map of Baft ophiolite mélange, modified from geological map of Sirjan, 1:250,000 [44]. b) Geological map of Baft ophiolite that is located between Sanandaj-Sirjan metamorphic zone and Ormieh-Dokhtar volcanic belt. c) Iranian ophiolites' distribution and location of studied ophiolite mélange in the map [3].

detailed study, notwithstanding the difficult task of deriving information from these complex rocks [33]. In this study, serpentinites from Baft ophiolite mélange were investigated and their genesis, tectonic setting and phase relations will be investigated by textures and chemical compositions of different types of spinels. Because mainly peridotites in this mélange have been deeply altered (serpentinized), primary minerals such as olivine and pyroxene have changed to secondary minerals. Spinel is only resistant primary mineral against alteration in these rocks. Because spinels are refractor phases and resist against alteration, they are reliable petrogenetic indicators [6], capable of recording

the magmatic history by which a fertile spinel lherzolite undergoes partial melting, producing basaltic melts and residual harzburgites [21]; Therefore detection of chemical composition of spinel in these rocks concerns particularly. Serpentinites from Baft ophiolite mélange contain different types of spinels which can reveal different stages of evolution in Baft serpentinites. The main scientific goal of this study is to provide a new perspective to aspects of the development of Baft ophiolite mélange based mainly on the chemical compositions and textural relationships of spinels in this mélange.
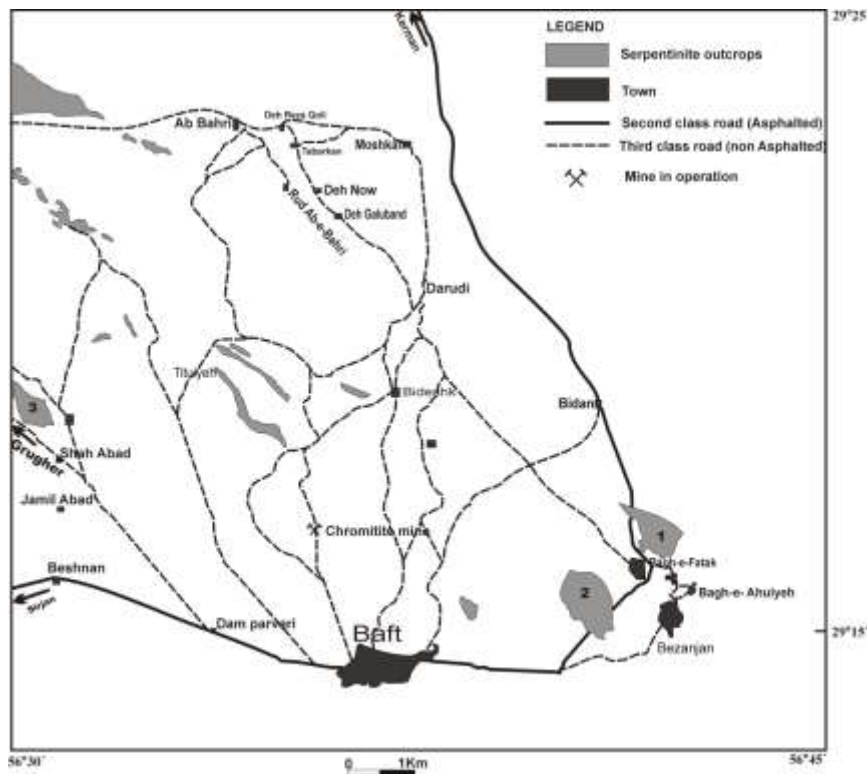
Figure 2. location of Gushk chromitite mine in serpentinite outcrops of Baft area
(Modified from Baft geological map of Iran, 1:100,000 series, [4]).

1. Geological Setting and Related Lithologies

Baft ophiolite mélange is a part of Naein-Baft ophiolite (south of Kerman province in Iran) (Fig. 1a) with length of 87.5 km and trend of northwest-southeast that has crop out along the major faults of Baft and Shahr-e-Babak. Geologically, Baft ophiolite mélange is located between Sanandaj-Sirjan metamorphic zone and Orumieh-Dokhtar volcanic belt (Fig. 1b). Serpentinites which hosted studied spinels are found as either big outcrops or as matrix that have surrounded other lithologies. In this ophiolite, there are lens-shaped chromitites that have surrounded by serpentinized dunites. Gushk mine is one of the largest chromitite mines in this ophiolite, located in southwest of Kerman province, 5km northwest of Baft city (Fig. 2) and this mine is investigated in the present work.

This ophiolite has studied by many authors and some of them believe that it represents a narrow, Red Sea–like ocean, created at a slow spreading center [e.g. 3]; or it is an arc basin related to Tethyan subduction [e.g. 18]; or a back-arc basin [42]. Three ^{40}Ar/^{39}Ar ages 101.2±0.9, 99.7±0.9, 99±1.2 Ma, for a hornblende gabbro, suggest an Upper Albian age for the generation of this ophiolite

[e.g. 18].

Baft ophiolite mélange consists of basalt (with pillow structure in some areas), serpentinized harzburgite and dunite, gabbro (both isotropic and layered), limestone patches, dolerites and minor diabasic dykes, pyroxenite veins, uniformly bedded radiolarian cherts and bedded pelagic limestones surrounded by schistose serpentinites. Veins of chromite ore bodies and little massive sulfides are also present. All lithological units in this mélange are strongly imbricated and sheared by closely spaced sub-vertical faults and shear zones. Structural complexities such as plentiful cracks, folds, tracks and veins are the most characteristic features in these serpentinites. These features indicate different phases of deformation which have affected on this area. In general, serpentinized harzburgites and dunites are the most dominate peridotites in this region that have undergone different degrees of serpentinazation. Harzburgites constitute approximately 70 vol. % of serpentinites and nowadays, they are seen as small blocks (several meters) to massive (several hundred meters) outcrops. Dunites constitute about 30 vol. % of the serpentinites, and their schistosity is more pervasive than the harzburgites.

25

2. Textural Characteristics of the Studied Serpentinized Peridotites

Pervasive metamorphism and subsequent alteration have substantially changed the primary petrographical and chemical characteristics of the peridotites. We were, however, able to identify the primary lithologies by the aid of relic textures. Peridotites in this ophiolite mélange contain olivine, orthopyroxene and minor clinopyroxene and Cr-spinel. Primary textures are granular and porphyroclastic, and the minerals show traces of mantle deformation. Based on their degree of serpentinization, the studied peridotites can be divided into three groups. (1) Those which have serpentinized up to 50 vol. % and the relics of fresh primary olivine and orthopyroxene can be seen. (2) Peridotites with 50-90 vol. % serpentinization, contain completely serpent-tinized olivine and relatively unaltered orthopyroxene. (3) Peridotites that have been serpentinized 90-100 vol. %. In this group, orthopyroxenes have bastitized and one can recognize them only with their pseudomorphic shapes. Main textures of olivine in the first and second groups are mesh, hourglass, banded-growth and polygonal, and texturally, these rocks are similar to serpentinites from southern Mariana forearc in Japan [47]. The first and second groups can be introduced by "mesh-textured serpentinite" term [12] containing ~90 vol. % serpentine (mostly lizardite and minor chrysotile veins), 10 vol.% orthopyroxene, 1-3% Cr-spinel and minor relics of olivine, diopside, talc, tremolite, ferritchromite and different types of veins (such as serpentine, magnetite, magnesite and talc veins).

In the third group rocks, antigorite is dominant and shows interpenetrative, interlocked, flare and blade textures. It has been overgrown on previous textures as vein or matrix. This group can be introduced by "flare-textured serpentinite" term [12] containing up to 90 vol. % serpentine (mostly antigorite) without any orthopyroxene or olivine and 1-3% Cr-spinel, talc, magnesite, chlorite, tremolite, ferritchromite and veins.

Materials and Methods

Studies on serpentinites from Baft ophiolite mélange include field, laboratories (microscopic and SEM) and geochemical (XRD and electron microprobe) studies. Scanning electron microscopy (SEM) was performed using LEO 1530 (EHT=15.00 kV, Mag=2.00KX, signal A=BSD) in Karlsruhe university of Germany. Chemical compositions of minerals were analyzed using a JEOL JXA 8900 SUPERPROBE electron microprobe at the University of Munster in Germany with an accelerating voltage of 15 kV and a current of 15 nA. Beam diameter

used was 5 μm. Elements analyzed are Si, Ti, Al, Fe, Mn, Mg, Ca, Na, K, Cr and Ni calculated on the basis of a set of natural and synthetic standards. In this study, chemical compositions of minerals that prepared on this area by Shafaii Moqadam [41] were used too.

Results

In serpentinites of Baft ophiolite mélange even in completely serpentinized rocks, we can just observe pesodomorphs of primary minerals (such as olivine or pyroxene), but precise studies of their pseudomorphs reveal primary textures in these rocks. In Fig. 3 from serpentinized harzburgites, orthopyroxene has been completely replaced by bastite, olivine has been completely serpentinized and shows hourglass and mesh texture. Crinkle boundary between orthopyroxene pseudomorph and Cr-spinel indicates that primary orthopyroxene and Cr-spinel have been grown contemporaneously. A chrysotile vein overprinted on them subsequently.

For a long time, spinels have been considered as petrogenetic indicators, capable of conveying information about magmatic features (melt composition, melting degree and crystallization pressure). In serpentinites of Baft ophiolite mélange, Cr-spinel grains mostly occur as irregular to idiomorphic shapes and most of them internally display three different zones: their core represents unaltered (primary) Cr-spinel, the intermediate zone correspond alteration of Cr-spinel to "ferritchromite" and the outer zone composed of evolved magnetite. Chlorite also occurs as thin rims surrounding altered Cr-spinel. Analyses that performed in unaltered cores have been used for petrogenetic purposes. Compositionally, four different types of spinels have been distinguished in the Baft serpentinites
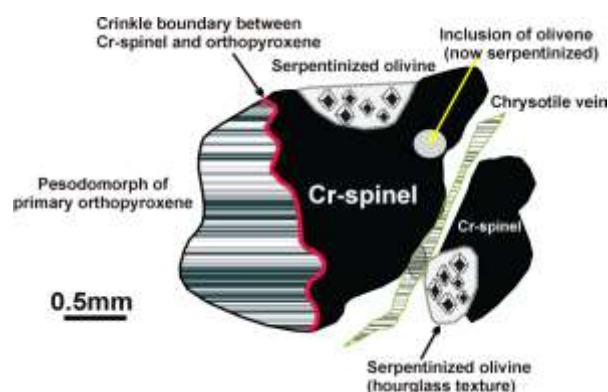

Figure 3. Schematic picture of primary textures in the Baft harzburgite after serpentinization.
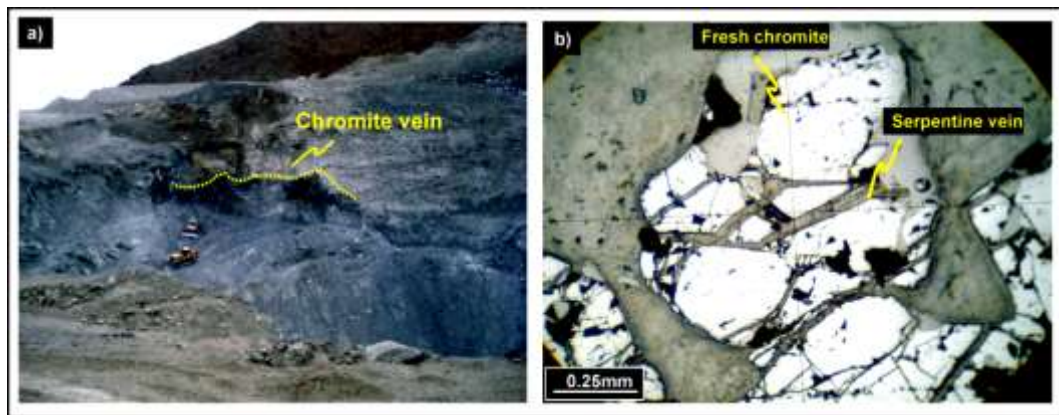
Figure 4. a) Gushk chromitite mines. The chromitites occur as pods with several meters thickness and their thickness increase with dept. b) Chromite grains in the studied chromitites. They are composed of aggregates of coarse-grained chromite crystals which have slightly altered along their grain margins (in reflex light).

as follows: (1) Chromite in massive chromitite deposits. (2) Disseminated primary Cr-spinel (including euhedral to subhedral, interstitial and vermicular spinels) in the peridotites. (3) Ferritchromite (with chlorite aureoles) that has developed on the primary Cr-spinels in serpentinized harzburgites. (4) Magnetite (type I and II) that has formed in the serpentinites.

1. Chromite in Massive Chromitites

Gushk chromite mine is one of the largest and the most important chromite mines of Iran that is located in southwest of Kerman province in 5km northwest Baft city (Fig. 2). This mine with 60 ton production per day is one of the most active chromite mines in Iran. Chromitite of this mine is the podiform type and forms separated layers or lens that have surrounded by serpentinized dunites. In some places, there are some layered type chromitites with several meters of thickness which increase in deeper levels. (Fig.4a). The length of chromitite lenses in dunites reaches up to 1 m and they show massive and disseminated textures. In many cases, the primary structures and textures of chromites have changed, but their chemical compositions can be used for genetic investigations. Chromitite lenses are composed of aggregates of coarse-grained chromite crystals which have slightly altered along their grain margins and cracks and serpentine vein have formed in them (Fig. 4b). Serpentine, talc and minor magnetite are common admixtures in the chromitite lenses. In some samples, the chromitite lenses show common textures and structures such as cumulate and banding, typical of magmatic crystallization.

1.1. Chemistry of Chromites

Chemical analyses of chromites for massive chromitites from Baft ophiolite are listed in Table 1. The studied chromites with average $Cr_2O_3=62.8\%$ and Cr#=0.83 [Cr#=Cr/(Cr+Al)] are Cr-rich chromitites and they are regarded as the first grade chromites in the world. In Cr_2O_3 vs. Al_2O_3 diagram (Fig. 5), these chromites plot in the field of podiform chromitite and with using Cr# and Mg# relations, (Fig. 6a-c and 7a-b) Baft chromitites belong to Alpine type deposits that have been crystallized from boninitic magmas. In Al_2O_3 vs. TiO_2 diagram from Kamenetsky et al. [25], these chromites plot in the suprasubduction zone field (Fig. 8a).

In Cr# vs. TiO_2 diagram (Fig. 8b) chromite compositions show an increase in TiO_2 at constant Cr#. This trend may have produced due to melt-mantle interactions [e.g. 10]. On the other hand, chromite compositions from Baft serpentinites have Al_2O_3 and TiO_2 contents similar to those from subduction related mantle peridotites and highly depleted MOR peridotites [25].

1.2. Parental Melt of Baft Chromitites

High Cr# values (Table 1) in Baft chromites (0.82-0.84) show that they have crystallized from boninitic magmas (as suggested by Tamura and Arai [46]). The plots of Cr# vs. Mg# (Fig. 6b-c and 7a-b) show that the primary chromite compositions are uniform and they plot in boninite field. Further insight into the chemistry of the parental melts for the studied chromites can be gained using the equation of Maurel and Maurel [32]:

Eq.1: Al_2O_3 wt% $_{chromite} = 0.035 (Al_2O_3)^{2.42}$ wt % $_{liquid}$

Table 1. Electron microprobe analyses of chromite from massive chromitite in the Baft ophiolite mélange. Analyses samples Bt06-41 prepared by Shafaii Moqadam et al. [41]

Sample	CH19	CH20	CH21	BT06-41	BT06-41	BT06-41	BT06-41	BT06-41	BT06-41	BT06-41	BT06-41	BT06-41
Lithology	Chr	Chr	Chr	Chr	Chr	Chr	Chr	Chr	Chr	Chr	Chr	Chr
SiO_2	0.05	0.04	0.01	0.00	0.00	0.03	0.02	0.03	0.02	0.00	0.00	0.00
TiO_2	0.14	0.18	0.19	0.15	0.11	0.18	0.14	0.21	0.15	0.16	0.15	0.14
Al_2O_3	8.68	9.24	8.32	7.99	7.83	7.87	7.98	8.06	8.32	8.02	8.01	7.93
Cr_2O_3	63.48	62.57	62.70	63.91	63.82	62.03	62.39	62.65	63.15	62.12	62.47	62.41
$FeO_{(t.)}$	14.96	14.55	14.67	13.97	14.11	14.86	14.97	15.24	14.21	15.58	15.30	15.38
MnO	0.27	0.29	0.32	0.00	0.00	0.00	0.00	0.00	0.00	0.00	0.00	0.00
MgO	15.13	15.21	15.03	13.55	13.65	13.66	13.74	13.42	13.73	13.77	13.69	13.59
CaO	0.03	0.02	0.02	0.00	0.00	0.00	0.04	0.00	0.00	0.00	0.01	0.00
NiO	0.15	0.18	0.08	0.09	0.08	0.07	0.15	0.14	0.10	0.10	0.09	0.08
Totals	102.89	102.30	101.35	101.07	101.14	100.44	101.16	101.33	101.47	101.83	101.58	101.58
Oxygen p.f.u	4.00	4.00	4.00	4.00	4.00	4.00	4.00	4.00	4.00	4.00	4.00	4.00
Si	0.00	0.00	0.00	0.00	0.00	0.00	0.00	0.00	0.00	0.00	0.00	0.00
Ti	0.00	0.00	0.01	0.00	0.00	0.00	0.00	0.01	0.00	0.00	0.00	0.00
Al	0.32	0.34	0.31	0.31	0.30	0.30	0.31	0.31	0.32	0.31	0.31	0.31
Cr	1.57	1.55	1.57	1.65	1.65	1.61	1.61	1.61	1.62	1.60	1.61	1.61
Fe^{3+}	0.10	0.10	0.11	0.04	0.05	0.07	0.07	0.06	0.05	0.09	0.08	0.08
Fe^{2+}	0.29	0.29	0.29	0.34	0.34	0.34	0.33	0.35	0.34	0.34	0.34	0.34
Mn	0.01	0.01	0.01	0.00	0.00	0.00	0.00	0.00	0.00	0.00	0.00	0.00
Mg	0.71	0.71	0.71	0.66	0.66	0.67	0.67	0.65	0.67	0.67	0.66	0.66
Ca	0.00	0.00	0.00	0.00	0.00	0.00	0.00	0.00	0.00	0.00	0.00	0.00
Ni	0.00	0.01	0.00	0.00	0.00	0.00	0.00	0.00	0.00	0.00	0.00	0.00
tot. cat.	3.00	3.00	3.00	3.00	3.00	3.00	3.00	3.00	3.00	3.00	3.00	3.00
Mg#	0.64	0.65	0.65	0.63	0.63	0.62	0.62	0.61	0.63	0.61	0.61	0.61
Cr#	0.83	0.82	0.84	0.84	0.84	0.84	0.84	0.84	0.84	0.84	0.84	0.84

Note: Cr# = [Cr/Cr+Al], Mg# = [Mg/Mg+Fe], FeO(t)= FeO + Fe_2O_3, Chr=Chromitite.

The results show that the contents of Al_2O_3 in chromitite parental melts are between 9.6-10.01% (Table 2). This value is similar to the Al_2O_3 contents of mid-ocean ridge and back-arc basin basalts [15]. Al_2O_3 values "between 9.11-11.6" are indicator of boninitic melts in suprasubduction zone [11].

2. Primary Disseminated Cr-Spinels

This group forms up to 3 vol. % of the harzburgites and include 3 types: The first one is euhedral to subhedral chromian spinels (Cr-spinels) (1-4mm size) that contain olivine (Fig. 9a), opx and cpx inclusions. Rarely, they show corroded areas with irregular shapes and sometimes altered to ferritchromite or magnetite along their cracks and boundaries. They usually show pull-apart cracks and the cracks have developed at right

angle to the long axes of grains (Fig. 9b). However existence of more than one set of fractures may be due to several deformation events (Fig. 9c). Sometimes, pull-apart cracks may be produced by serpentinazation of surrounding silicate phases or inclusions. In these cases when olivine serpentinized, pull-apart cracks show a radial pattern (Fig. 9d).

The second type is small grain interstitial spinel (up to 0.5 mm) which has developed between other grains (Fig. 9e). This type of spinel is more altered than the former and has frequently been surrounded by beard antigorite.

The third type is vermicular spinels which have been grown with olivine or pyroxene simultaneously (Fig. 9f). In this texture, olivine usually altered and removed, and spinel has remained with vermicular shape. Occasionally, vermicular spinels are surrounded by

beard or massive antigorite. Probably, antigorite is formed as a result of another stage of deformation. In this case, spinel has acted as a porphyroclast and antigorite has developed around it. In the studied rocks, Cr-spinels are very resistant against deformation and as seen in Fig. 10a a resistant Cr-spinel grain causes to curvature of layered lizarditic vein. Fig. 10b also shows a euhedral Cr-spinel in contact with three veins, none of the veins could penetrate into the Cr-spinel. Around of this crystal, beard antigorite have developed subsequently.

Cr-spinel is the only mineral from the original ultramafic rock that regularly retains its original igneous composition after serpentinization. In completely serpentinized ultramafic rocks, the composition of unaltered spinel is extensively used as a petrogenetic indicator [e.g. 2, 6, 13, and 24]. Chemical analyses of disseminated Cr-spinels from Baft serpentinites are listed in Table 3. Compositional variations of these spinels is shown in Fe^{3+}-Al^{3+}-Cr^{3+} triangle diagram (Fig. 11a). Cr_2O_3 and Al_2O_3 values in the primary Cr-spinel change between 38.90-42.90 wt. % and 25.51- 29 wt. % respectively. Cr_2O_3 and Al_2O_3 are negatively correlated and are plotted in mantle array (Fig. 11b). In these minerals, the Cr# contents range between 0.46-0.53 (Table 3) and Mg# values change between 0.56 - 0.67. In the harzburgites, Mg# contents are limited [30, 36] and in the studied area, this rang is placed between 0.56-0.67. However, Mg# is strongly affected by the amount of silicate phases in these rocks [13]. FeO contents in Cr-spinels range between 16.5 and 18.2 wt. %; while TiO2 (<0.16 wt. %), MnO (<0.29 wt. %), and NiO (<0.2 wt. %) values are low.

Generally, ferric iron contents in the Cr-spinels are very low, and in Figure 11c, Fe^{3+} shows a negative relation to Cr and Al. In this diagram, with increasing alteration, Fe^{3+} is replaced by Al^{3+} and Cr^{3+}. In TiO2 vs. Cr# diagram (Fig. 11d), the harzburgitic Cr-spinels plot in the "depleted peridotite field" because of small amounts of TiO2. These features show that the harzburgites represent residual rocks that basaltic or Mg-rich andesitic magmas have been extracted from them [2]. Based on Table 3 and Fig. 11b-d, Cr-spinels in Baft ophilite malange are refractory spinels and their hosted peridotites have been formed by partial melting of spinel lherzolite protoliths in the pressure of 10–20 kbar [20].

In Cr# vs. TiO2 diagram, all of disseminated Cr-spinels from Baft ophiolite plot in abyssal peridotite array because they have lower TiO2 content than the Baft chromites (Fig. 8b). Also in Cr-Al-Fe^{3+} triangle diagram, all of the harzburgitic samples plot in the abyssal peridotite array (Fig. 12) and in Cr# vs. Mg#

diagram (Fig. 6a-c), the residual harzburgitic protoliths plot in the field of Alpine type peridotites.

3. Ferritchromite Rims and Chlorite Aureoles

Alteration products after Cr-spinel in the studied area contain ferritchromite, magnetite, chlorite and or kammererite. Replacement of Cr-spinel by ferritchromite starts along its fractures and progressively affects the sub-grains of Cr-spinel (Fig. 13a). The volume of replacement changes from sample to sample (e.g., increasing from Fig. 13a to 13e). The presence of kammererite indicates that in these minerals, chromium has been released from Cr-spinels and Fe enters into the chlorite structure, where Cr substitutes for Al [35].

Ferritchromite rims are usually surrounded by irregular and colorless aureoles of chlorite up to 3 mm in thickness (Fig. 13f). The formation of chloritic aureoles around ferritchromite can be described in three stages. Dissolution of Cr-spinels giving rise to ferritchromite rims in the first stage. Then, Mg and Al release during the alteration of primary Cr-spinel and interact with surrounded serpentine in mesh textures producing chlorite aureoles. The formation of chlorite through spinel alteration has been described by Kimball [27] as a high-T process (> 400°C) in presence of MgO

Table 2. Average Al_2O_3 (wt. %) contents ratio of melts in equilibrium with the accessory chromite in serpentinite from Baft ophiolite

	$Al_2O_3^{(1)}$	Reference
Baft ophiolite	9.11-11.16	This study
Tehuitzingo chromitites	15.30	Proenza et al. [39]
Boninite	10.6-14.4	Wilson [49]
MORB	16.00	Wilson [49]
Back-arc basin basalts	>16.0	Fryer et al. [15]

Note: ($^{(1)}$Maurel and Maurel [32]. $^{(1)}Al_2O_3$ wt% $_{chromite}$ = 0.035 $(Al_2O_3)^{2.42}$ wt % $_{liquid}$).
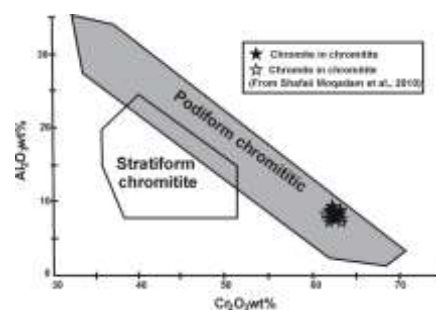

Figure 5. Cr_2O_3 vs. Al_2O_3 diagram [8].The studied chromites plot in "podiform chromitite" array.
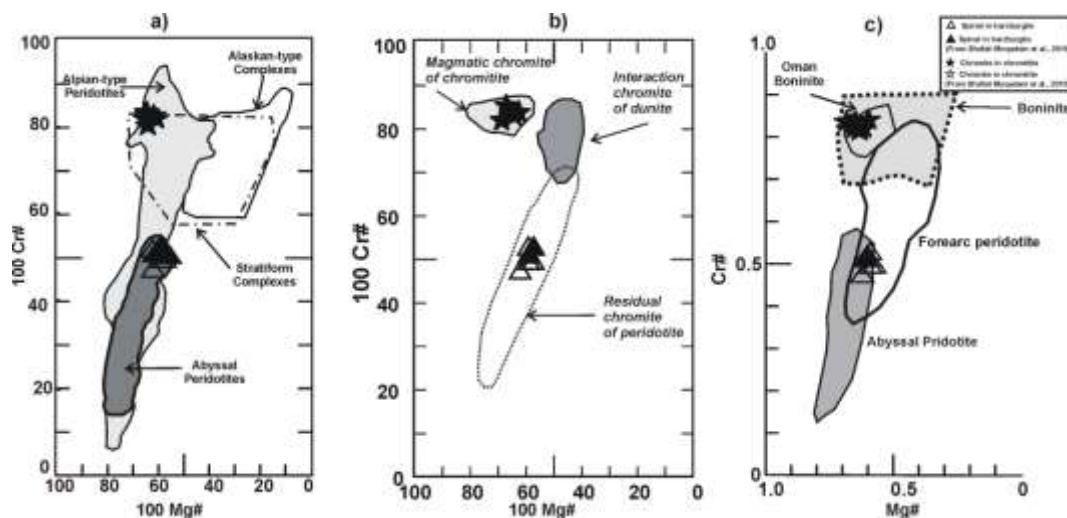
29

Figure 6. Relationship between Mg# and Cr# of primary spinel in different tectonic settings: a) Fields for abyssal peridotites and Alpian-type peridotites are after Dick and Bullen [13]. b) Fields for residual, magmatic and interaction of chromite are after Zouh et al. [50]. c) The fore-arc peridotite field is defined based on data from Bloomer and Fisher [7], Pearce et al. [38].
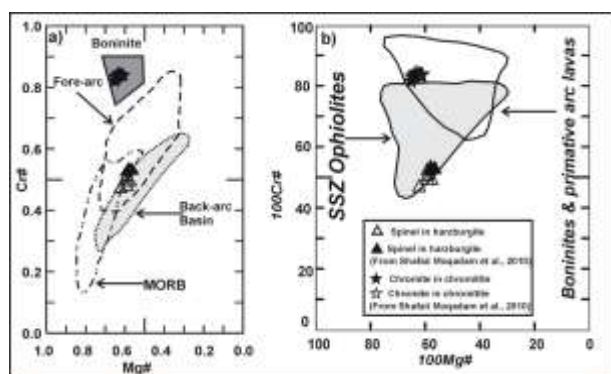

Figure 7. Plots of primary spinel in Baft serpentinites: a) Cr# vs. Mg# diagram for unaltered spinels (after Stern et al. [45]). The field boundaries are from Dick and Bullen [13] and Ohara et al. [37]. b) Cr# vs. Mg# diagram for Baft spinels. Supra-subduction zone (SSZ) peridotites field and boninite and primitive arc lava field are from Bridges et al. [9].
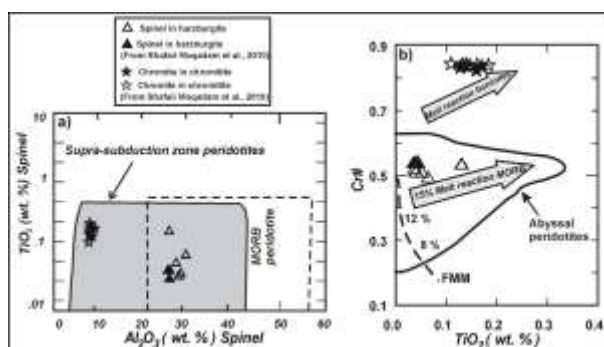

Figure 8. a) Al_2O_3 vs. TiO_2 diagram from Kamenetsky et al. [25] in spinel of the Baft serpentinites. b) Plots of primary spinel in the Baft serpentinites in Cr# vs. TiO_2 diagram. Arrows indicate effects of MORB melt reaction on refractory abyssal peridotite spinels and boninite melt reaction on refractory suprasubduction zone peridotite spinels [10]. FMM = Fertile MORB Mantle.

and SiO_2 rich fluids, according to the following reaction:

Eq. 2: $Mg\,Al_2\,O_4 + 4\,MgO + 3\,SiO_2 + 4\,H_2O \rightarrow Mg_5\,Al\,Si_3\,Al\,O_{10}\,(OH)_8$
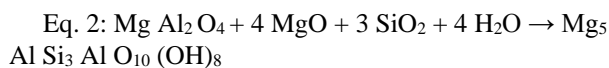
But Mellini et al. [33], suggest two stages for the formation of chlorite in this environment.

The first one corresponds to the replacement of the primitive spinel by the ferritchromite. The second one affects the outer mesh serpentine, which is progressively transformed to a disordered chlorite/lizardite intergrowth.

The formation of ferritchromite in turn leads to an increase in dissolved chromium, which is in conjunction with ferric iron, results in the precipitation of numerous fine-grained ferritchromites and magnetites [23] (Eq. 3):

Eq. 3: Cr-Spinel + Fe^{+3} + $H_2O \rightarrow$ Ferritchromite + Fe_3O_4 + Al^{+3} + H_2
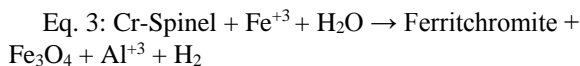
Excess Al reacts with serpentine minerals to produce chloritic aureoles. Aluminum released during alteration of Cr-spinel is associated with intergrowth of clinochlore and serpentine and formed crinkle rim in Cr-
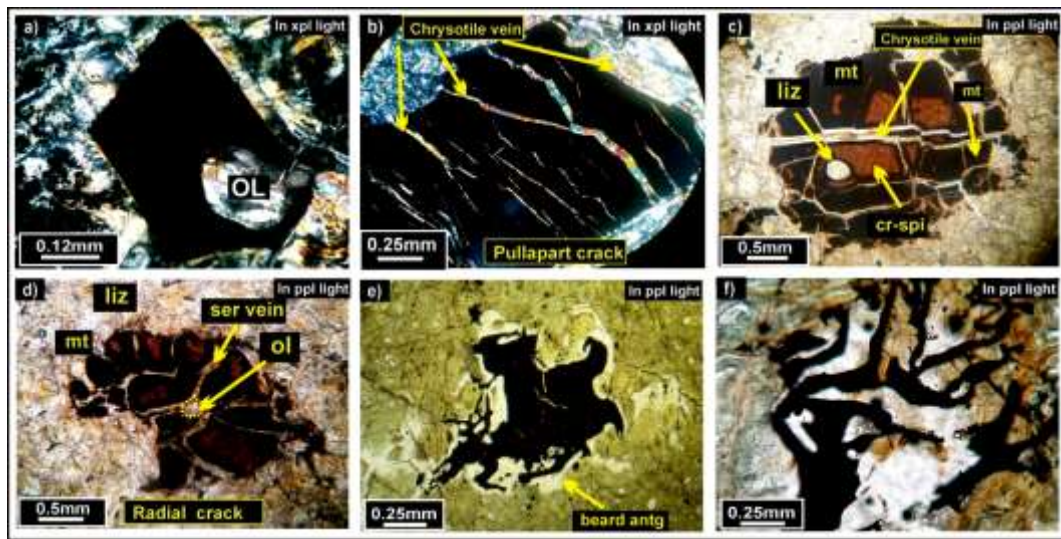
Figure 9. Representative serpentinite textures of Baft ophiolite: a) Idiomorphic Cr-spinel with olivine inclusion. b) Pull-apart crack texture in a coarse Cr-spinel. c) Two set of fractures in a Cr-spinel grain. d) Radial cracks duo to serpentinization of olivine inclusion. e) Interstitial spinel that surrounds with beard antigorites (bright in color). f) Spinels with vermicular texture that surround with beard antigorite. (OL:olivine, mt:magnetite, liz:lizardite, spi:spinel, ser:serpentine, antg:antigorite).
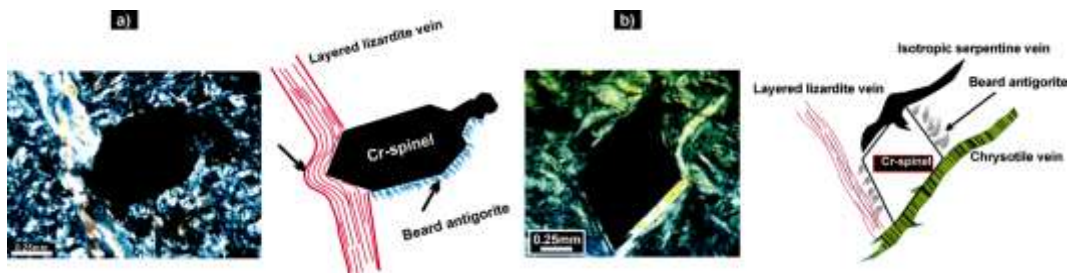

Figure 10. Euhedral Cr-spinels that have resisted against deformation in studied harzburgite: a) Permanence of Cr-spinel versus a layered lizarditic vein which it causes to curvature of vein. b) Euhedral Cr-spinel that has made contact with three veins (layered lizarditic vein, isotropic serpentine vein and chrysotile vein) and none of the veins could penetrate into Cr-spinel.

spinel [23, 33, 47] (Eq. 4):

Eq. 4: $Al^{+3} + (Mg,Fe)_3Si_2O_5(OH)_4 + H_2O \rightarrow (Mg,Fe,Al)_{5-6}(Si,Al)_4O_{10}(OH)_8 + H^+$
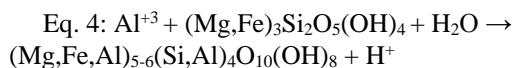
Chlorite aureoles overgrowth mesh textures indicate that chlorite formed after main serpentinization. However, it is mentioned [33] that serpentinization process produces the rims of secondary magnetite around chromite, and this opens the possibility that ferritchromite may be formed by regional metamorphism of these rimmed grains [19]. Mellini et al. [33] also suggest that after the main serpentinization, Cr-spinels are progressively replaced by ferritchromite rims by a dissolution–recrystallization process.

4. Magnetite

Secondary magnetites are less attending but in studied rocks, magnetite is a key implement with great important in order to detecting conditions of serpentinization. It has made of up to 10% modal percent of some serpentinites in the samples. Two generations of magnetite can be recognized in studied rocks: (1) syn-serpentinization magnetite (Type I) and (2) post-serpentinization or recrystallized magnetites (Type II).

Syn-serpentinization magnetites have formed during initial static serpentinization of peridotites probably in ocean floor setting. This generation is found in mesh-textured serpentinites and divides into 4 groups:

Table 3. Electron microprobe analyses of Cr-spinel in the serpentinized harzburgites of the Baft ophiolite mélange. Analyses samples Bt06-28 prepared by Shafaii Moqadam et al. [41]

Sample	H23	H26	H38	H71	H72	H73	Bt06-28	Bt06-28	Bt06-28
Lithology	Hz	Hz	Hz	Hz	Hz	Hz	Hz	Hz	Hz
SiO_2	0.01	0.06	0.01	0.00	0.01	0.07	0.00	0.03	0.00
TiO_2	0.16	0.07	0.03	0.04	0.03	0.05	0.03	0.04	0.04
Al_2O_3	25.51	29.16	26.57	28.05	27.62	27.07	25.55	25.55	25.21
Cr_2O_3	41.80	38.40	42.11	40.44	42.24	38.91	42.83	42.86	42.90
$FeO_{(t.)}$	18.22	17.22	14.90	18.14	17.43	16.50	17.25	16.52	16.70
MnO	0.21	0.29	0.19	0.29	0.24	0.18	0.28	0.19	0.28
MgO	14.77	15.83	17.68	13.72	14.08	13.27	12.48	12.66	12.88
CaO	0.03	0.00	0.03	0.00	0.01	0.05	0.05	0.06	0.01
NiO	0.20	0.13	0.21	0.11	0.07	0.10	0.00	0.12	0.16
Totals	101.04	101.19	101.76	100.79	101.76	96.22	98.51	98.18	98.17
Oxygen p.f.u	4.00	4.00	4.00	4.00	4.00	4.00	4.00	4.00	4.00
Si	0.00	0.00	0.00	0.00	0.00	0.00	0.00	0.00	0.00
Ti	0.00	0.00	0.00	0.00	0.00	0.00	0.00	0.00	0.00
Al	0.90	1.00	1.36	0.98	0.96	0.99	0.93	0.93	0.92
Cr	0.99	0.88	0.58	0.95	0.99	0.96	1.04	1.05	1.05
Fe^{3+}	0.11	0.11	0.07	0.07	0.05	0.05	0.03	0.01	0.03
Fe^{2+}	0.34	0.31	0.28	0.39	0.38	0.38	0.42	0.41	0.40
Mn	0.01	0.01	0.00	0.01	0.01	0.01	0.01	0.00	0.01
Mg	0.66	0.69	0.72	0.61	0.62	0.62	0.57	0.58	0.59
Ca	0.00	0.00	0.00	0.00	0.00	0.00	0.00	0.00	0.00
Ni	0.01	0.00	0.01	0.00	0.00	0.00	0.00	0.00	0.00
tot. cat.	3.00	3.00	3.00	3.00	3.00	3.00	3.00	3.00	3.00
Mg#	0.59	0.62	0.68	0.57	0.59	0.59	56.32	57.73	57.90
Cr#	0.52	0.47	0.30	0.49	0.51	0.49	52.93	52.84	53.30

Note: Hz=Harzburgite, Cr#=Cr/(Cr+Al), Mg#=Mg/(Mg+Fe2), FeO(t)=FeO + Fe_2O_3.

(a) This group contains those magnetites that have formed simultaneously with serpentinazation of olivine. During this process, additional iron forms fine-grained magnetites along the fractures and forms magnetite slim veins too (Fig. 14a-b).With re-infiltration of fluids into the fractures and further serpentinization, lizardite grows toward the core of olivine grains. This process repeats until no olivine remains or involved fluid consumes. Multi-stage growth of lizardite produces a structural zoning in these rocks. This zoning has been characterized by magnetite veins (Fig. 14b). Moreover, these magnetite veins show fluid passageways. Sometimes, relics of olivines in the core of the mesh textures, have been affected by new stage of serpentinization and serpentine-magnetite aggregates produced. In these cases, the patterns of magnetite grains indicate the shape of serpentine crystals (Fig. 14c). Indeed, this group of magnetites could show original fractures in olivine grains (Fig. 14a and d).

(b) This group contains magnetites that have been formed during serpentinazation of pyroxenes. They can show original mantle deformation features and cleavages of the pyroxenes. During bastittization of orthopyroxene, fine grains of magnetites are produced as thin rings around the orthopyroxene (Fig. 14e and 15a). Fig. 15b also shows thin veins of magnetite that have been formed along the primary curved cleavages and indicate curvature and intense deformation produced by mantle conditions.

(c) Third group contains magnetite veins that have been formed during formation of chrysotile fibers. These veins with up to 1 cm in thickness have
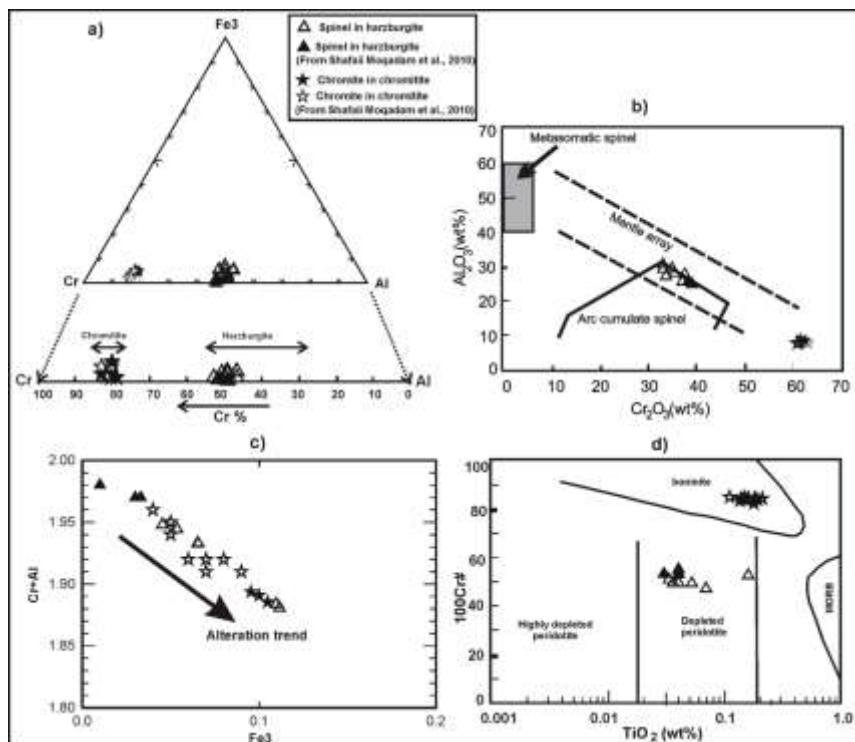
Figure 11. a) Chemical compositions of studied spinels on triangle diagram Fe^{3+} - Al^{3+} -Cr^{3+}. b) Negative correlation between Cr_2O_3 and Al_2O_3 in studied spinels that plot in mantle array (fields after Haggerty [20]). c) Clear negative relation between Fe^{3+} and Cr+Al. d) Cr# vs. TiO_2 diagram for the analyzed accessory unaltered spinels. Cr-spinels in harzburgite samples plot in "depleted peridotite field" and chromites plot in "boninite" (Fields after Dick and Bullen [13] and Arai [2]).

crystallized simultaneously with the formation of chrysotile and magnetite. They follow the shape and growth style of chrysotile fibers.

(d) Fourth group contains magnetites that have formed due to Cr-spinel alteration. This group forms along the fractures or cracks or around the Cr-spinel grains (Fig. 14f).

Post-serpentinization magnetites or type II have probably formed after main serpentinization process. This generation is found in flare-textured serpentinites and divides into two groups; the first group contains irregular or idiomorphic magnetites that have formed in veins or as idiomorphic shapes around Cr-spinels or on the matrix (Fig. 16a and b respectively). Second group contains magnetites that have formed during formation of antigorite in dynamic metamorphism. These magnetites follow growth style and shape of antigorite fibers (Fig. 16c-f) and so, they can help for investigation of genesis of antigorite fibers.

Discution

In textural point of view, the studied rocks can be divided into two groups: "mesh-textured serpentinites" and "flare-textured serpentinites". It seems that flare-textured serpentinites have been subjected to higher temperature and pressure condition, and their formation
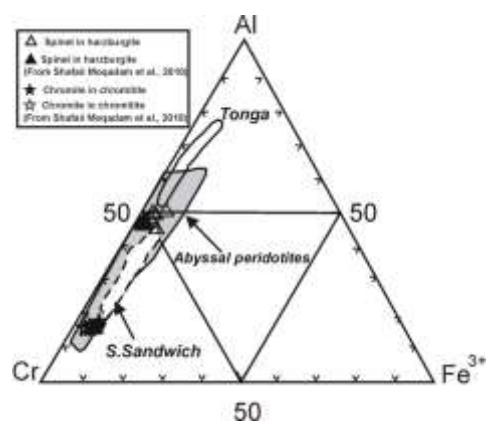

Figure 12. Trivalent cation ratios in chromian spinel from peridotite xenoliths from the mantle wedge. Field for abyssal peridotites is from Tamura and Arai [46] and field Tonga arc is from Bloomer and Fisher [7].
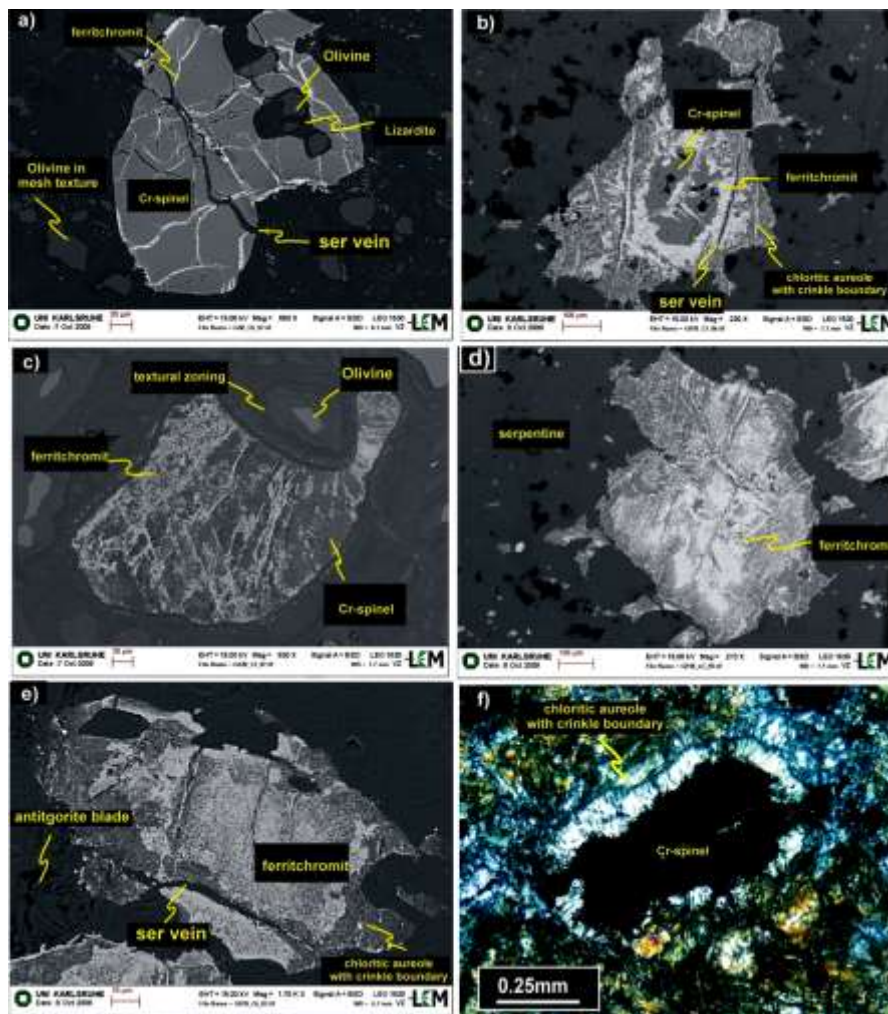
Figure 13. SEM images of different Cr-spinels with variable alteration (alteration increases from a-e). Cr-spinel crystal affected by intense fracturing and partially replaced by ferritchromite (the bright rims) and Cr-spinel is surrounded by a chloritic aureole (dark part). f) ferritchromitic Cr-spinel with chlorite aureole in xpl light (ser:serpentine).
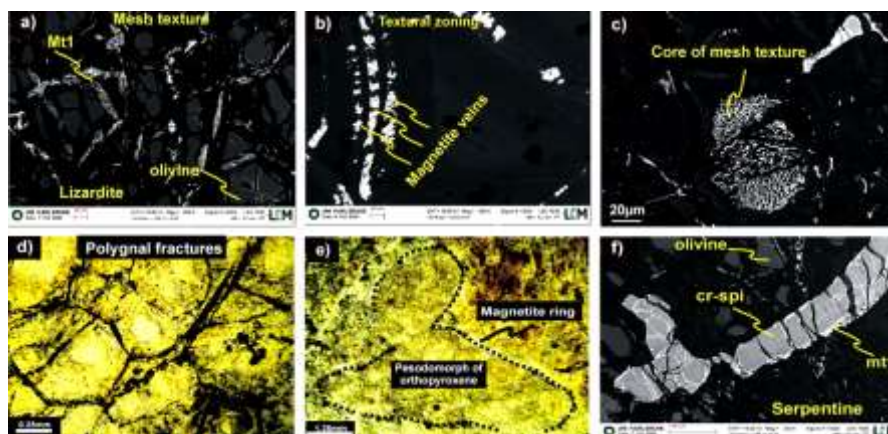

Figure 14. Different types of syn-serpentinization magnetites (Type I). a-d) Magnetites which have been formed due to the olivines' serpentinization (first group). e) Magnetites that have simultaneously formed with serpentinazation of pyroxene (second group). f) Magnetites that have formed after Cr-spinel alteration (forth group). mt1: Magnetites of Type I (first generation).

cannot be related to static alteration of peridotites in the ocean floor setting [34]. According to Shahabpour [42] and Ghasemi and Talbot [17] the studied area is a part of Naein-Baft oceanic lithosphere, so, flare-textured serpentinites with different degrees of serpentinization may has been formed by subduction of this oceanic lithosphere beneath central Iranian microcontinent. The formation of interpenetrative and interlocked antigorites, can be related to this procces or uplift of serpentinized pridotites in another time (as stated by González-Mancera et al. [19] for Tehuitzingo serpentinites in Acatlan Complex, SW Mexico). It seems that the studied lizardite and chrysotile are the result of static alteration in an ocean floor environment, while interpenetrative-blade antigorites have been formed due to dynamic metamorphism.

In the studied area, many Cr-spinels have been replaced by ferritchromite and a lizardite-chloritic aureole surrounds the both. On compositional fields for chlorites and serpentines (Table 4) (Fig. 17) [14, 22], serpentine minerals in the matrix, plot in the serpentine area, while aureole chlorites (around Cr-spinel) plot in the penninite $[(Mn,Al)_6(Si,Al)_4O_{10}(OH)_8]$ field.

1. Genesis of Secondary Magnetites

As mentioned above, different types of magnetites can be found in the Baft serpentinite. There are some considerations about the genesis of them as follows:

In peridotites, as pressure decreases and volume increases, regular, irregular or polygonal fractures create in olivine grains. With alteration of olivine and formation of lizardite along its fractures during entrance of fluids, mesh, hourglass, polygonal or banded-growth textures produce. The site of the original fractures in the olivine may be marked as mesh rims [48] and a string of magnetite grains. Magnetite is a common mineral phase within the mesh serpentinites and with increasing of serpentinization, olivines alter and serpentine and magnetite are replaced olivines according following reaction [47]:
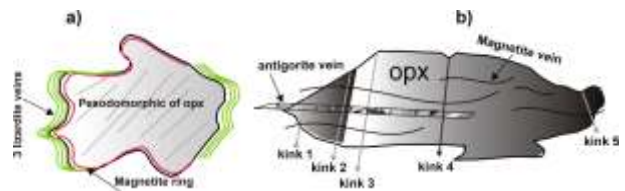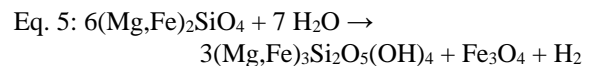
Eq. 5: $6(Mg,Fe)_2SiO_4 + 7 H_2O \rightarrow$
$$3(Mg,Fe)_3Si_2O_5(OH)_4 + Fe_3O_4 + H_2$$

Figure 15. Schematic pictures of magnetites that have simultaneously formed with orthopyroxene serpentinazation in Baft serpentinized harzburgites. a) Formation a magnetitic rim around orthopyroxene and preservation of original shape of orthopyroxene. b) Formation of magnetitic veins along primary cleavages of orthopyroxene (kink:kink band).
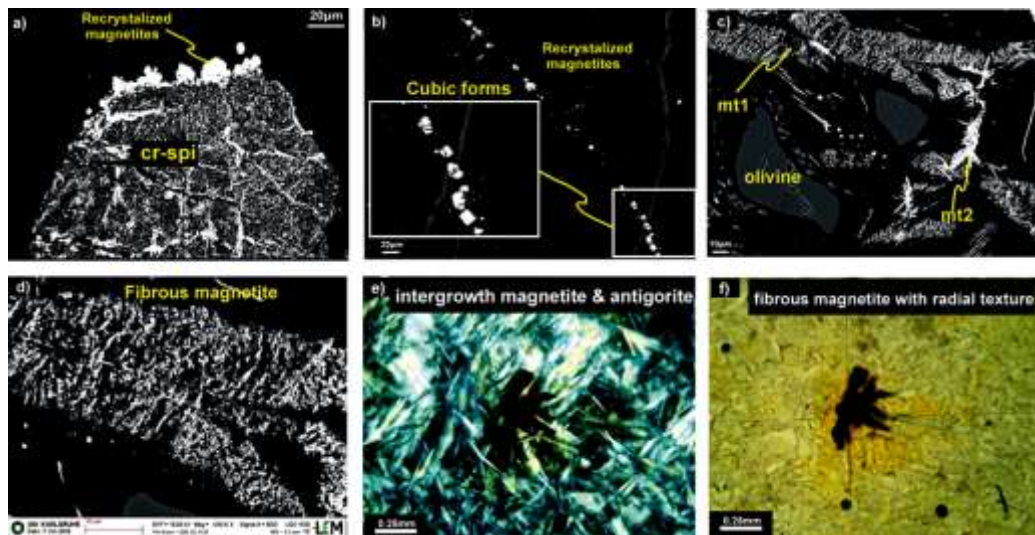
Figure 16. Types of post-serpentinization magnetites (Type II). a) Formation of recrystallized magnetite as idiomorphic forms around the primary Cr-spinel. b) Development of magnetite with cubic form on the serpentinitic matrix. c) Fibrous magnetite that has simultaneously developed with growth of antigorite in serpentinized matrix (mt2). d) Fibrous magnetite that has simultaneously developed with growth of antigorite in vein. e) Intergrowth of magnetite and antigorite with radial texture. f) Shows "e" figure in ppl light. mt1: Magnetites of Type I (first generation), mt2: Magnetites of Type II (second generation).

Table 4. Representative electron microprobe analyses of serpentine minerals and chlorite in serpentinites from Baft ophiolite mélange

Sample	H9	H34	H36	H51	H76	D45	H47	H77	H80	D12	D10	D11
Lithology	Hz	Hz	Hz	Hz	Hz	Hz	Hz	Hz	Hz	Hz	Hz	Hz
SiO_2	40.67	43.49	43.72	41.23	39.4	40.9	43.84	42.29	41.96	43.72	31.57	30.81
TiO_2	0.022	0.000	0.000	0.000	0.030	0.012	0.000	0.000	0.000	0.000	0.000	0.000
Al_2O_3	0.429	0.476	0.441	0.261	1.96	3.08	0.297	0.278	0.387	0.00	0.00	0.026
Cr_2O_3	0.00	0.532	0.018	0.00	1.022	0.263	0.027	0.198	0.03	0.00	0.00	0.00
FeO	8.12	4.89	4.47	6.73	3.19	3.53	3.63	2.86	4.48	3.64	26.3	29.03
MnO	0.142	0.082	0.066	0.086	0.104	0.06	0.203	0.075	0.069	0.031	0.233	0.263
MgO	33.45	37.28	38.56	33.36	36.94	37.3	37.45	39.29	38.02	39.93	29.32	28.07
CaO	0.262	0.083	0.016	0.06	0.111	0.032	0.047	0.071	0.056	0.085	0.087	0.07
Na2O	0.00	0.015	0.00	0.054	0.00	0.00	0.00	0.011	0.00	0.00	0.064	0.061
K2O	0.016	0.016	0.022	0.022	0.012	0.026	0.012	0.00	0.028	0.00	0.025	0.031
NiO	0.523	0.149	0.195	0.203	0.291	0.268	0.194	0.552	0.48	0.066	0.044	0.092
Totals	83.635	87.013	87.509	82.005	83.06	85.471	85.701	85.625	85.51	87.472	87.644	88.453
Oxygen(p.f.u)	7.00	7.00	7.00	7.00	7.00	7.00	7.00	7.00	7.00	7.00	7.00	7.00
Si	2.06	2.082	2.067	2.118	1.956	1.973	2.118	2.026	2.029	2.053	1.615	1.58
Ti	0.001	0.00	0.00	0.00	0.001	0.00	0.00	0.00	0.00	0.00	0.00	0.00
Al	0.026	0.027	0.025	0.016	0.115	0.175	0.017	0.016	0.022	0.00	0.00	0.002
Fe^{3+}	0.00	0.00	0.00	0.00	0.00	0.00	0.00	0.00	0.00	0.00	0.779	0.846
Cr	0.00	0.02	0.001	0.00	0.04	0.01	0.001	0.008	0.001	0.00	0.00	0.00
Fe^{2+}	0.344	0.196	0.177	0.289	0.132	0.142	0.147	0.115	0.181	0.143	0.346	0.399
Mn	0.006	0.003	0.003	0.004	0.004	0.002	0.008	0.003	0.003	0.001	0.01	0.011
Mg	2.526	2.66	2.718	2.555	2.733	2.683	2.698	2.807	2.741	2.796	2.236	2.146
Ca	0.014	0.004	0.001	0.003	0.006	0.002	0.002	0.004	0.003	0.004	0.005	0.004
Ni	0.00	0.001	0.00	0.005	0.00	0.00	0.00	0.001	0.00	0.00	0.006	0.006
Na	0.001	0.001	0.001	0.001	0.001	0.002	0.001	0.00	0.002	0.00	0.002	0.002
K	0.021	0.006	0.007	0.008	0.012	0.01	0.008	0.021	0.019	0.002	0.002	0.004
tot.cat.	5.00	5.00	5.00	5.00	5.00	5.00	5.00	5.00	5.00	5.00	5.00	5.00
Mg#	0.88	0.931	0.939	0.898	0.954	0.95	0.948	0.961	0.938	0.951	0.665	0.633

Note: Analyses D10-D11 are prepared from the points around Cr-spinel in chlorite aureole (Mg# = [Mg/(Mg+Fe)], Hz=Harzburgite).

As chemical composition of olivine goes toward fayalite, the formation of magnetite veins enhances too. Therefore, first group of magnetites could show original fractures in olivine grains (Fig. 14a and d) or rims or core of the mesh texture (Figs. 14a and 14c).

During bastitization of orthopyroxene, additional iron forms fine grains of magnetites as thin rings around orthopyroxene. This type can show original shape and cleavages in serpentinized pyroxenes in Baft serpentinites. The original orthopyroxene in serpentinites of the Eastern Desert in Egypt also is indicated by the presence of bastite texture with very thin magnetite streaks that define cleavage planes of the original orthopyroxene [29, 35].

In the studied area, some of magnetites have been formed simultaneously with chrysotile. These fibrous chrysotiles have crystallized in different veins. One of

these veins is crack-seal type and has filled by fibrous chrysotile crystals. Crack-seal is a mechanism proposed to explain the formation of veins showing banding, made for example by wall or fluid inclusions [1]. This mode of formation consists in an incremental opening followed by complete sealing of small successive cracks [40]. Because successive cracks are very thin, chrysotile fibers in these cracks are very thin and short, so it is difficult to recognize the shape, size and genesis of them. In this case, secondary magnetites are useful criteria for showing the genesis of chrysotile.

Some of magnetites have been formed due to the alteration of Cr-spinel. The formation of magnetite in order to an increase in dissolved chromium, which is in conjunction with ferric iron, results in the precipitation of fine-grained magnetite.
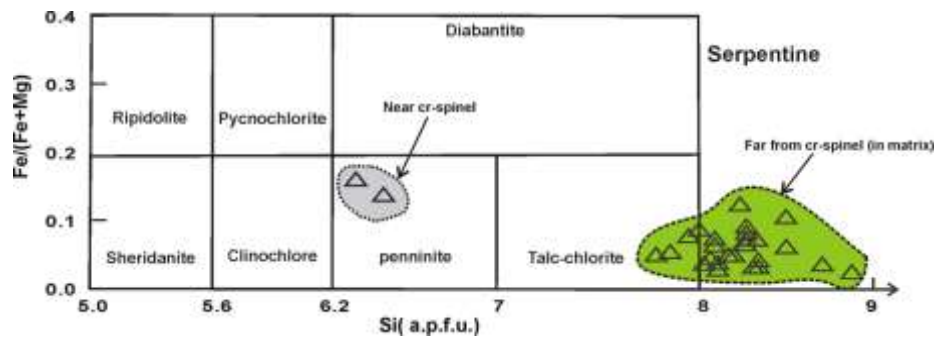
Probably post-serpentinization magnetites have

Figure 17. Compositions of 'chlorite/serpentine' from the Baft serpentinites. Chlorite classification diagram has adapted from Hey [22]. Serpentine filed is from Facer et al. [14].

formed after main serpentinization or in dynamic metamorphism conditions as follow:

Irregular or idiomorphic magnetites have produced in different stages of deformation and since their shapes are idiomorphic, it is most probably that they crystallized from Fe-rich fluids. Growth of idiomorphic magnetite along the void's walls indicates precipitation from aqueous fluid, rather than from gas alone [43]. Open-space filling and brecciation suggest that fluid pressures were locally higher than lithostatic pressure [26]. Orientation of the Fibrous magnetite toward the vein center (Fig. 16c-f) may indicate their growth from the walls toward the vein center. Distortion of magnetite fibers or folding in serpentine veins along the central plane (Fig. 16c-d) indicates that the formation of magnetite was accompanied by deformation. The relation of serpentine (antigorite) enclosing fine magnetite crystals, and vice versa, indicates that all of them were precipitated from the same fluid simultaneously [16].

The fibrous and idiomorphic habits of magnetite, respectively, were strongly controlled by interrelated variables such as diffusion rate of involved components, growth rate of involved minerals, temperature, degrees of supersaturation and viscosity of involved fluids [e.g. 28]. Various evidences show that in Baft serpentinites, magnetites have been originated by different reactions in the peridotites such as proposed by Barnes [6] and Gahlan et al. [16].

Generally, the concentration of Fe as magnetite veins is associated by adding magnetite component in chromian spinel upon alteration. Iron released from olivine on serpentinization could enrich chromian spinel with magnetite component. In ordinary serpentinized peridotites, the Fe released from olivine was precipitated as in situ fine discrete magnetite particles. The source of iron was internally supplied from olivine upon serpentinization. The mineralizing hydrothermal fluids utilized shears cracks and tension joints for transportation and precipitation of iron, which transported as ferrous hydroxide [16].

2. Tectonic Setting of Baft Ophiolite Mélange

Many evidences show that the Baft ophiolite has formed in a suprasubduction zone in an arc/back-arc environment (Fig. 7a-b and 8a). Moreover, on the Cr# vs. Mg# diagram (Fig. 7a), unaltered disseminated Cr-spinels mainly plot in the back-arc field. The higher values of Cr# in these minerals positively correlate with the degree of partial melting. As stated by Dick and Bullen [13], Cr-spinels become richer in Cr with increasing degrees of depletion .The Cr# values of Cr-spinels from Baft serpentinite is less than 0.6, whereas, in fore-arc peridotites this value is more than 0.65 and reaches up to 0.85 [13]. In Al_2O_3 vs. TiO_2 diagram (fig. 8a) [25] studied peridotites plot in suprasubduction zone peridotite field too.

3. Conclusion

- It seems that in the studied area, flare-textured serpentinites have passed higher temperature and pressure conditions. It is probably that they have been resulted from dynamic forces inserted by subduction of Naein-Baft oceanic slab beneath central Iranian microcontinent; but mesh-textured serpentinites have been formed by static metamorphism in ocean floor environments.

- The compositions of Baft chromites show they are Alpian type and podiform chromitites and they have crystallized from boninite magma in a suprasubduction zone environment probably. It seems that the Baft chromite ores initially have been formed in a primary ophiolite complex within dunitic layers. Due to serpentinization of ultramafic parts and due to the

activity of serpentinite diapirs in next stages, the deposits have been emplaced into the upper crust shear zones.

- The compositions of primary disseminated Cr-spinels show that the Baft ophiolite has been formed in a suprasubduction zone in an arc/back-arc environment. And the host rocks are mantle residual harzburgites (Alpian type peridotite).

- The studies suggest that after the main serpent-tinization, Cr-spinels are progressively replaced by ferritchromite rims. Probably, alteration of magmatic spinel to "ferritchromite" in Baft serpentinites is a product of regional metamorphism.

- Chlorite aureoles that have been grown on the mesh textures indicate that chlorites have formed after main serpentinization.

- There are two generations of magnetites in Baft serpentinites: Type I or syn-serpentinization and Type II or post-serpentinization. Probably type I have formed during initial static serpentinization in ocean floor and type II have formed after main serpentinization or during dynamic metamorphism.

Acknowledgments

References

1. Andreani, M., Baronnet, A., Boullier, A.M. and Gratier, J.P. A microstructural study of a "crack-seal" type serpentine vein using SEM and TEM techniques. European Journal of Mineralogy **16**: 585-595 (2004).
2. Arai, S. Chemistry of chromian spinel in volcanic rocks as a potential guide to magma chemistry. Mineralogical Magazine **56**: 173-184 (1992).
3. Arvin, M. and Robinson, P.T. The petrogenesis and tectonic setting of lavas from the Baft ophiolitic mélange, southwest of Kerman, Iran. Canadian Journal of Earth Sciences **31**: 824–834 (1994).
4. Baft geological map of Iran. 1:100,000 series, sheet **7348** (1972).
5. Barnes, S.J. Chromite in Komatiites, II. Modification during greenschist to mid-amphibolite facies metamorphism. Journal of Petrology **41**: 387–409 (2000).
6. Barnes, S.J. and Roeder, P.L. The range of spinel compositions in terrestrial mafic and ultramafic rocks. Journal of Petrology **42**: 2279–2302 (2001).
7. Bloomer, S.H. and Fisher, R.L. Petrology and geochemistry of igneous rocks from the Tonga trench, a non-accreting plate bound- ary. Journal of Geology **95**: 469–495 (1987).
8. Bonavia, F.F., Diella, V. and Ferrario, A. Percambrian podiform chromitites from Kenticha Hill Southern Ethiopia. Economic Geology **88**: 198-202 (1993).
9. Bridges**,** J.C., Prichard, H.M. and Meireles, C.A. Podiform chromitite-bearing ultrabasic rocks from the Bragança massif, Northern Portugal: fragments of island arc mantle?. Geological Magazine **132**: 39–49 (1995).
10. Choi, S.H., Shervais, J.W. and Mukasa, S.B. Suprasubduction and abyssal mantle peridotites of the coast range ophiolite, California. Contributions to Mineralogy and Petrology **156**: 551-576 (2008).
11. Crawford, A.J., Falloon, T.J. and Green, D.H. Classification, petrogenesis and tectonic setting of boninites. In: Crawford, A.J. (ed.) Boninites and Related Rocks. London: Unwin Hyman p.1-49 (1989).
12. Dengo, C., and Logan, J. Implications of the Mechanical and Frictional Behavior of Serpentinite to Seismogenic Faulting. Journal of Geophysical Research **86**(B11): 10771-10782 (1981).
13. Dick, H.J.B. and Bullen, T. Chromian spinel as a petrogeneticindicator in abyssal and alpine-type peridotites and spatiallyassociated lavas. Contributions to Mineralogy and Petrology **86**(1): 54–76 (1984).
14. Facer, J., Downes, H. and Beard, A. In situ Serpentinization and Hydrous Fluid Metasomatism in Spinel Dunite Xenoliths from the Bearpaw Mountains, Montana, USA. Journal of Petrology **50**: 1443-1475 (2009).
15. Fryer, P., Taylor, B., Langmuir, C.H. and Hochstaedter, A.G. Petrology and geochemistry of lavas from the Sumisu and Torishima backarc rifts. Earth and Planetary Science Letters **100**: 161-178 (1990).
16. Gahlan, H.A., Arai, S., Ahmed, A.H., Ishida, Y., Abdel-Aziz, Y.M. and Rahimi, A. Origin of magnetite veins in serpentinite from the Late Proterozoic Bou-Azzer ophiolite, Anti-Atlas, Morocco: An implication for mobility of iron during serpentinization. Journal of African Earth Sciences **46**: 318–330 (2006).
17. Ghasemi, C.J. and Talbot. A new tectonic scenario for the Sanandaj–Sirjan Zone (Iran). Journal of Asian Earth Sciences **26**: 683–693 (2006).
18. Ghazi, A.M., and Hassanipak, A.A. Petrology and geochemistry of the Shahr-Babak ophiolite, Central Iran, in Dilek Y., Moores E.M., Elthon D., and Nicolas A., eds., Ophiolites and Oceanic Crust: New insight from field and the Ocean Drilling Program. Geological Society of America Special Paper **349**: 485–497 (2000).
19. González-Mancera, G., Ortega-Gutiérrez, F., Proenza, J.A. and Atudorei, V. Petrology and geochemistry of Tehuitzingo serpentinites (Acatlan Complex, SW Mexico). Boletin de la Sociedad Geologica Mexicana **61**(3): 419-435 (2009).
20. Haggerty, S.E. Upper mantle opaque mineral stratigraphy and the genesis of metasomatites and alkali-roch melt. Journal of Geological Society Australia **14**: 687-699 (1988).
21. Hellebrand, E., Snow, J.E., Dick, H.J.B. and Hofmann, A.W. Coupled major and trace elements as indicators of the extent of melting in mid-ocean-ridge peridotites. Nature **410**: 677-681 (2001).
22. Hey, M.H. A new review of the chlorites. Mineralogical

Magazine **30**: 277-292 (1954).

23. Iyer, K., Austrheim, H. and John, T. Serpentinization of the oceanic lithosphere and some geochemical consequences: constraints from the Leka ophiolite complex, Norway. Chemical Geology **249**: 66–90 (2008).

24. Jaques, A.L. and Green, D.H. Anhydrous melting of peridotite at 0-15 kb pressure and the genesis of tholeii,tic basalts. Contributions to Mineralogy and Petrology **73**: 287-310 (1980).

25. Kamenetsky, V.S., Crawford, A.J. and Meffre, S. Factors controlling chemistry of magmatic spinel: an empirical study of associated olivine, Cr-spinel and melt inclusions from primitive rocks. Journal of Petrology **42**: 655–671 (2001).

26. Kent, A.J.R., Ashley, P.M., and Fanning, C.M. Metasomatic alteration associated with regional metamorphism: an example from the Willyama Supergroup, South Australia. Lithos **54**: 33–62 (2000).

27. Kimball, K.L. Effects of hydrothermal alteration on the composition of chromian spinels. Contributions to Mineralogy and Petrology **105**: 337–346 (1990).

28. Kirkpatrick, R.J., 1975. Crystal growth from the melt: a review. American Mineralogist 60, 798–814.

29. Khalil, A.E.S., Azer, M.K. Supra-subduction affinity in the Neoproterozoic serpentinites in the Eastern Desert, Egypt: Evidence from mineral composit. Journal of African Earth Sciences **49**: 136–152 (1975).

30. Leblanc, M. and Nicolas, A. Ophiolitic chromitite. International Geology Review **34**: 653–686 (1992).

31. Matsumoto, I. and Arai, S. Morphological and chemical variations of chromian spinel in dunite–harzburgite complexes from the Sangun zone (SW Japan): implications for mantle/melt reaction and chromitite formation processes. Mineralogy and Petrology **73**: 305–323 (2001).

32. Maurel, C., Maurel, O. Etude experimental de la distribution de l'aluminiun entre bain silicate basique et spinelle chromifere. Implications petrogenetiques: tenure en chrome des spineless. Bulletin de Mineralogie **105**: 197-202 (1982).

33. Mellini, M., Rumori, C. and Viti, C. Hydrothermally reset magmatic spinels in retrograde serpentinites: formation of ''ferritchromit'' rims and chlorite aureoles. Contributions to Mineralogy and Petrology **149**: 266–275 (2005).

34. Mohammadi, N. Mineralogy, seismicity and petrogenesis of serpentinites in ChoharGonbad-Gugher-Baft coloured mélange in Kerman province. MSc thesis, Shahid-Bahonar University of Kerman, Iran. p. 225 (2010).

35. Mokhles, K. Azer, and Robert, J. Stern. Neoproterozoic (835–720 Ma) Serpentinites in the Eastern Desert, Egypt: Fragments of Forearc Mantle. Journal of Geology **115**: 457–472 (2007).

36. Mysen, B. O. and Kushiro, I. Composiotin of variation of co-existing phases with degree of melting of peridotite in the upper mantle. American Mineralogist **82**: 52-67 (1977).

37. Ohara, Y., Stern, R.J., Ishii, T., Yurimoto, H., and Yamazaki, T. Peridotites from the Mariana Trough: First look at the mantle beneath an active back-arc basin. Contributions to Mineralogy and Petrology **143**: 1–18 (2002).

38. Pearce, J.A., Barker, P.F. and Edward, S.J. Geochemistry and tectonic significance of peridotites from the South Sandwich arc-basin system, South Atlantic. Contributions to Mineralogy and Petrology **139**: 36-53 (2000).

39. Proenza, J.A., Ortega-Gutiérrez, F., Camprubí, A., Tritlla, J., Elías-Herrera, M. and Reyes-Salas, M. Paleozoic serpentinite-enclosed chromitites from Tehuitzingo (Acatlán Complex, southern Mexico): a petrological and mineralogical study. Journal of South American Earth Sciences **16**: 649-666 (2004).

40. Ramsay, J.G. The crack-seal mechanism of rock deformation. Nature **284**: 135-139 (1980).

41. Shafaii Moghadam, H., Robert, J. Stern, and Rahgoshay, M. The Dehshir ophiolite (central Iran): Geochemical constraints on the origin and evolution of the Inner Zagros ophiolite belt. Geological Society of America **122**: 1516–1547 (2010).

42. Shahabpour, J. Tectonic evolution of the orogenic belt in the region located between Kerman and Nwyriz. Journal of Asian Earth Science **24**: 405-417 (2005).

43. Sillitoe, R.H., Burrows, D.R. New field evidence bearing on the origin of the El Laco magnetite deposits, northern Chile. Economic Geology **97**: 1101–1109 (2002).

44. Sirjan geological map of Iran. 1:250,000 series. No: **I11** (1995).

45. Stern, R.J., Johnson, P.R., Kro¨ner, A. and Yibas, B. Neoproterozoic ophiolites of the Arabian-Nubian Shield. In Kusky T.M., ed. Precambrian ophiolites and related rocks. Dev. Precambrian Geology **13**: 95–128 (2004).

46. Tamura, A., Arai, S. Harzburgit-dunite-orthopyroxenite suite ophiolite mantle. Lithos **90**: 43-56 (2006).

47. Wang, X., Zeng, Z. and Chen, J. Serpentinization of peridotites from the southern Mariana forearc. Progress in Natural Science **19**: 1287–1295 (2009).

48. Wicks, F.J., Whittaker, E.J.W. and Zussman, j. An idealized model for serpentine textures after olivine. Canadian Mineralogist **15**: 446-458 (1977).

49. Wilson, M. Igneous petrogenesis: London, U.K., Unwin Hyman: 466 p (1989).

50. Zouh, M.F., Robinson, P.T., Malpas J. and Li Z. Podiform chromitites in the Luobusa ophiolite (SouthernTibet): implications for melt-rock interaction and chromite segregation in the upper mantle. Journal of Petrology **37**: 3-21 (1996).